Geomechanics for Energy and the Environment 36 (2023) 100494

Contents lists available at ScienceDirect

Geomechanics for Energy and the Environment

journal homepage: www.elsevier.com/locate/gete

Landslide susceptibility evaluation in Alpine environment: 2. Thermo-hydro-mechanical modeling for the response to climate-related variables

Andrea Morcioni [a,*], Tiziana Apuani [a], Francesco Cecinato [a], Manolis Veveakis [b]

[a] Università degli Studi di Milano, Dipartimento di Scienze della Terra "Ardito Desio" via Mangiagalli 34, 20133 Milano, Italy
[b] Duke University, Civil and Environmental Engineering Department, Durham, NC, USA

ARTICLE INFO

Article history:
Received 2 June 2023
Received in revised form 30 August 2023
Accepted 30 August 2023
Available online 9 September 2023

Editors-in-Chief:
Professor Lyesse Laloui and Professor Tomasz Hueckel

Keywords:
Thermo-hydro-mechanical modeling
Shear band
Thermal sensitivity

ABSTRACT

This paper is Part 2 of two companion papers, proposing a multidisciplinary approach to assess stability and velocity evolution of a large landslide located in the Central Italian Alps (upper Valtellina region): the Ruinon landslide. Part 1 of this work presented a 3D stress–strain finite element analysis, which assessed the morphological and geomechanical predisposition of the slope to gravitational instabilities and defined the current stress state along the slope. In this paper, a thermo-hydro-mechanical (THM) numerical analysis is applied to the landslide shear zone, to assess the link between landslide driving factors and the shear band material response. Data used as input for the model were pore pressure, reference stresses and initial temperature at the sliding surface, as well as the monitored velocity of the landslide body, assumed to move as a rigid block. The shear band material was modeled as a visco-plastic medium with thermal softening and velocity hardening, thus thermal- and load-rate sensitivity of the material were estimated through laboratory testing. To this end, triaxial compression tests with thermal control were performed on rock samples representative of the shear band. To constrain the model, results of the analysis presented in Part 1 were used to define the stress state at the sliding surface and the relationship between pore pressure and shear stresses. Then, pore pressure data from in-situ piezometers relevant to the period 2014–2018 were introduced and a best fitting between modeled and monitored landslide velocities was obtained. Finally, velocities were forecasted for the period 2018–2020 and a process of validation was performed using field displacement data. The outputs of the model adequately simulate the measured landslide velocity, reproducing the sliding behavior and its relationship with pore pressure. The presented approach may be applied to further case studies, aimed at defining a novel physics based early warning strategy for landslides.

1. Introduction

Large slope instability processes are the result of a complex interaction among different geological, geomorphological, and climatic factors. Their evolution can lead to catastrophic events (i.e., slope collapse) with a great impact on human activities, causing destruction and loss of life. Even if a slope collapse is not achieved, episodic acceleration of large landslides can cause infrastructure damage and lead to secondary gravitational events such as rockfalls and debris flows. Because of their great socio-economic impact, in the last decades, several studies have been developed to understand their causes, behavior, and create tools to predict their evolution over time and space.

Analytical, statistical, and numerical methods have been deployed to understand the long-term evolution of such natural processes, predicting stability, future displacements, and potential catastrophic scenarios. Some authors (e.g.,[1–6]) have focused on the evolution of mobilizing stresses (i.e., climatic, seismic and anthropic factors) and their interaction with internal resisting forces through the concept of limit equilibrium, leading to the calculation of slope's factor of safety. However, this approach does not allow to calculate the displacement evolution, and has limited validity in a three-dimensional time-dependent system. This concept was progressively replaced with real-time deformation assessment tools, firstly suggested by Saito 1965 and Saito 1969[7,8] and generalized by Voight 1988.[9] These tools are based on the definition of the landslide collapse time, by calculating the inverse of the measured velocity: when the inverse of velocity reaches zero (i.e., displacement tends to infinity), the landslide accelerates catastrophically, representing slope failure.[10,11] While these methods are effective for the development of real time early warning systems, they are not able to forecast the activation of the slope movement and displacement, as they neither include

* Corresponding author.
E-mail address: andrea.morcioni@unimi.it (A. Morcioni).

https://doi.org/10.1016/j.gete.2023.100494

physical nor geometrical factors (e.g., material properties and landslide geometries).

In this context, stress–strain models can be developed to analyze the relationship between external (e.g., climate, seismic events, human activities) and internal factors (e.g., mechanical properties, slope morphology). They are able to reproduce site-specific conditions, allowing to evaluate landslide initiation mechanisms and simulate the induced displacement field.[12–18] Stress–strain models are usually focused on analyzing the mechanisms of initial onset of failure and their topographic, geological and climatic control.[19–21]

The time-dependent evolution of large landslides is usually accounted for, by introducing a creep behavior of the slope.[22,23] The typical creep deformation curve consists of three distinct stages in a strain-time diagram: (i) primary or transient creep, (ii) secondary or steady-state creep, (iii) tertiary or accelerating creep. Following the initial stage with high strain rates, slip continues at a sustained long-term steady rate, due to the evolution of drainage conditions, thermal softening, and a rate-strengthening slip behavior of the shear zone.[24] For higher shear stresses, the development of microcracks and cavities leads to increased porosity and reduced effective contact area between material components, resulting in higher strain rates. When increased pore pressure reduces the effective stress, causing further loss of shear strength, accelerated creep can occur, leading to catastrophic failure.

In recent years, several authors focused on the time-dependent behavior of landslide shear band materials.[25–29] Understanding the behavior of the sliding surface and its response during slip, is, in fact, key to analyze and predict the failure mechanisms of deep-seated landslides. Veveakis et al. 2007[30] developed a model applied to the Vajont landslide, that accounts for heat production due to sliding friction in the shear band, relating the creeping motion to a thermally self-driven transient process. This creeping phase can be followed by progressive heating localization within the shear band that eventually triggers a catastrophic pressurization phase. Cecinato and Zervos 2012[31] proposed a generalized constitutive model accounting for heat generation and diffusion, pore pressure generation and dissipation, and thermal dependence of shear band materials, suitable to capture the final collapse dynamic evolution of large-scale landslides occurring in a coherent fashion. De Blasio and Medici 2017[32] studied the material response of the shear band due to friction and temperature increase related to acceleration steps of a sliding mass.

Considering all the above evidence, Seguí et al. 2020[33] provided a time-dependent assessment tool for large deep-seated landslides, combining internal and external factors acting on their sliding surface. This model assumes that the landslide body may be represented by a rigid block sliding on a thin visco-plastic shear band, undergoing thermal softening and velocity hardening. When the landslide moves, mechanical dissipation, due to friction, raises the basal temperature, while the shearing resistance of the shear-band material is reduced. This process can continue up to the point that when the shear strength decreases uncontrollably, due to a thermal runaway instability,[34] considering the history of external loading conditions that weakens the shearing resistance of the sliding surface. Based on a number of experimental studies conducted on clayey material,[35] that showed a dependence of mechanical properties on temperature[36,37] and loading rate,[38,39] Seguí and Veveakis 2021[35] performed further laboratory tests on landslide shear band materials, demonstrating their thermal and loading rate sensitivity, also constraining the model assumptions.

In this work, the 1D thermo-poro-mechanical mathematical model proposed by Seguí et al. 2020[33] and Seguì 2020[40] is applied to the Ruinon landslide, located in the Central Italian Alps (upper Valtellina region). Ruinon represents one of the most active cases in the Alpine region, with a main sliding surface located at a depth of 70–90 m, for a total estimated volume of the sliding mass of about 20 Mm^3.[41–43] The aim of this study is to implement a physically based model, that will allow to forecast the stability and the velocity evolution of the landslide, by providing critical values for measurable variables (i.e., groundwater level). This study explores the capabilities of an innovative tool for analyzing the landslide evolution, which accounts for thermal and velocity sensitivities of the shear band material, as well as the effect of pore pressure, in promoting the evolution of different creep stages.

The present work represents 'Part 2' of an analysis introduced in a companion paper, Morcioni et al. 2023,[44] where a numerical Finite Element Model (FEM) was defined to simulate the current stress–strain state of the Ruinon slope. The results of the FEM modeling will be used to define the stress state at the slip surface of the landslide, as well as the distribution of pore pressures.

The paper is structured as follows. First, the Ruinon landslide is described focusing on the main geological features and its driving factors. Then, based on collected data from the landslide monitoring system and laboratory tests conducted on rock samples, the implementation of a thermo-poro-mechanical model is described. Next, a process of calibration is performed using data relevant to the period 2014–2018, followed by a validation analysis regarding the 2018–2020 period. Results from the numerical analyses are finally presented focusing on the simulated strain and velocity evolution of the landslide.

2. Ruinon landslide

The Ruinon landslide is located in the Upper Valtellina region (Central Italian Alps), between the villages of Bormio and Santa Caterina Valfurva, on the right flank of the Frodolfo Valley (Fig. 1). This landslide is considered one of the most active cases in the Alpine region, with a main sliding surface located at a depth of approximately 70–90 m, for a total estimated volume of the sliding mass of 20 Mm^3.[41–43] The main active body extends at elevations between 1600 and 2100 m a.s.l., and is located at the toe of a deep-seated gravitational slope deformation (Saline DSGSD), which affects the entire slope up to its top at 3000 m a.s.l.[19,45] Two different landslide scarps identify the main active body: the so-called "high niche", which develops between about 2050 and 2100 m a.s.l., and the "low niche", located at 1900–1950 m a.s.l. (Fig. 1); the two rock scarps have considerable heights, of the order of tens of meters. Direct geological investigations conducted by the authors of this work confirm the main geomorphological features noted by previous studies[19]: above the landslide body, traction trenches, tensile fractures, scarps and structural depressions approximately parallel to the main valley axis (predominantly in the WNW-ESE direction) are present, indicating a strong gravitational activity of the slope (Fig. 1).

The geological framework is related to the Austroalpine Nappe arrangement composed by a crystalline basement of the Pre-Permian age. Along the slope, the "Bormio Phillites", a metapelitic unit belonging to the Campo nappe outcrops (Fig. 1), with a pervasive millimetric schistosity and mylonitic texture.[46,47] The outcropping rock masses are highly fractured and strongly deformed with isoclinal and minor transposed folds recording a polyphase tectonic and metamorphic evolution during the Varisican and Alpine orogenies.[48–50] The Ruinon slope is affected by brittle tectonic activity, as shown by the presence of faults, generally sub vertical or steeply inclined, connected to recent distension processes. Three main systems of brittle structures with ENE-WSW, NNE-SSW, and NE-SW directions are present (Fig. 1). In particular, the last one (NE-SW) outcrops along the main axis of the landslide body.

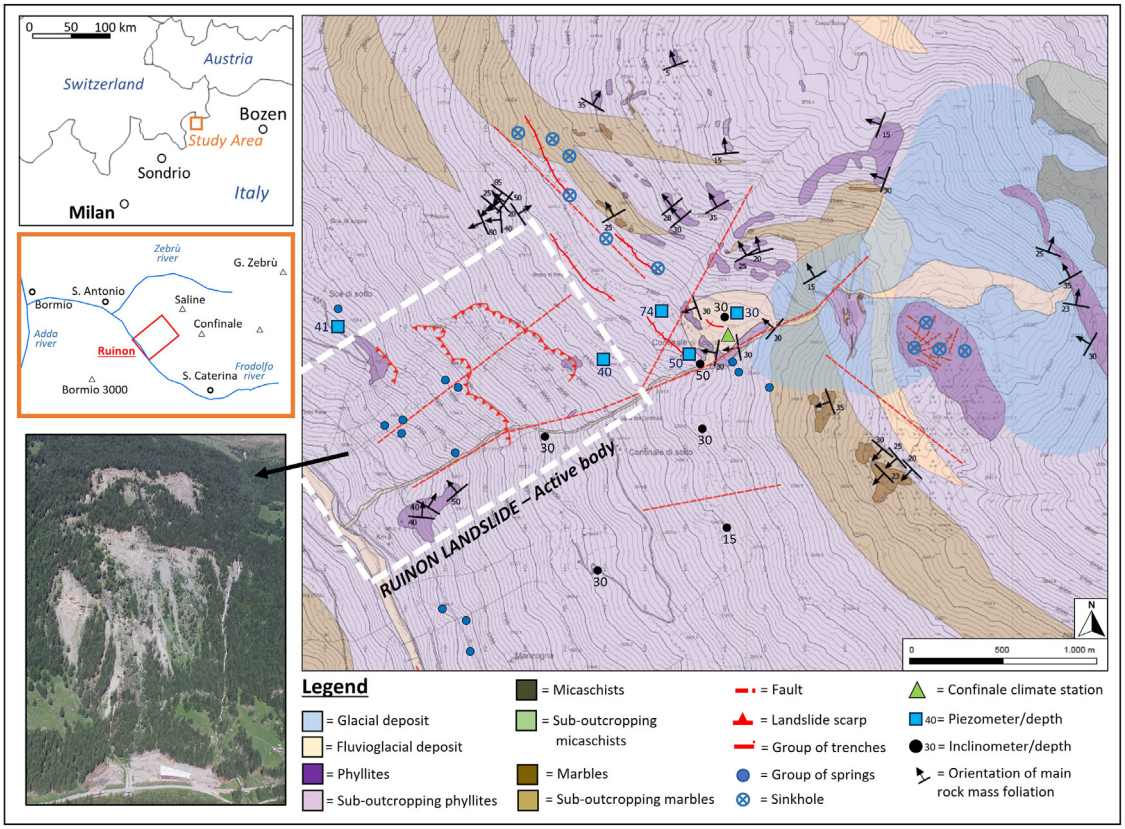

Fig. 1. Geological settings of the Ruinon landslide.

Due to the intense gravitational activity and surface weathering processes, the active landslide body consists of strongly disoriented phyllite boulders of the size of meters to decameters in diameters, embedded in a silty matrix. A large deposit of debris covers the entire slope, down to the bottom of the valley.

Geotechnical and seismic surveys allowed to define the nature of the rock-mass below the landslide deposit, showing a lithological uniformity with extremely fractured phyllites lying on undisturbed phyllites. Boreholes drilled in 1988–1989, identified a deep shear zone of gravitational origin characterized by up to 2 meters thick layers of cataclastic granular material and a highly weathered silty matrix. They were defined by a sudden drop of the RQD (Rock Quality Designation) index, with values tending towards zero within the undisturbed phyllites body.[42] The installation of inclinometers allowed to highlight the presence of secondary composite surfaces affecting the debris cover. However, many uncertainties remain with regards to the deep pattern of deformation since inclinometers have been sheared off quickly after installation, due to the high activity of the shallower debris. The presence of multiple weak layers, highlight that significant internal differential movements could exist from the sliding base up to the surface.

The slope exhibits a complex hydrogeological setting governed by the presence of the Confinale stream, flowing on the left flank of the landslide body. The presence of multiple traction elements, such as morphological depressions and sinkholes, promote surface water infiltration upstream of the main landslide body (Fig. 1). In addition, sub-vertical faults along both the Confinale stream and the landslide body, could significantly affect deep water circulation. Previous authors recognized the presence of an aquifer located within the landslide body due to the high permeability material (debris and highly disarticulated rock masses) laying over a silty low-permeability layer, corresponding to the sliding surface. However, groundwater circulation and aquifer recharge system are not well understood yet. Downstream of the lower niche, two spring alignments at 1850 and 1750 m a.s.l. are present (Fig. 1). Their location could be connected to the emergence of the slip surface.

By previous studies[41–43,51,52] it has been recognized that pore water pressures highly influence the activity of the landslide. Analysis of displacement-time and velocity–time behavior showed impulsive landslide acceleration events when the piezometric level rises, which are superimposed on slow and constant slope movements. A key role of rainfall and snowmelt as an accelerating factor for the landslide has been observed[41] with accelerations primarily occurring in late spring to summer.

2.1. Landslide evolution

Even if the local name “Ruinon” (meaning ruined slope) reveals a persistent instability of the slope, no gravitational events in the area were reported before 1960. The landslide has been showing intense activity since 1981, and it experienced a major acceleration in 1987–1988 due to heavy rainfall that affected the entire region (Valtellina floods). In 1984, following the occurrence of debris flows, the first geological investigations were carried out, and in 1997, after severe rockfalls, an in-situ monitoring network was installed.

Slope hazards related to the evolution of the landslide threaten the national road SS300, that runs through the valley bottom connecting the villages of Bormio and Santa Caterina Valfurva. A major risk is that a general collapse could obstruct the Frodolfo River, creating an unstable dam that would be potentially hazardous for villages along the valley. In June 1998, a debris flow interrupted the national road, and a monitoring system was implemented (see Section 2.2) and upgraded to an automated mode.

Between spring 2014 and fall 2016, accelerated displacements led to frequent road closures because of a possible progression of the sliding mass downslope of the lower scarp. In June 2019, landslide velocities increased to much higher values than ever before, reaching more than 1 m/day for 5 months.[52] Although a failure of the rockslide still did not occur, a great amount of debris moved downstream reaching the valley floor. A rock block of about 90 m^3 rolled down, damaging the national road, and forcing its prolonged closure. The most active areas in recent years have been the central and western parts of the lower body, and new scarps developed in the northwest portion. After the 2019 events, important actions concerning the improvement of passive structures to protect the National Road and reduce the risk of flooding, in case of collapse, have been carried out. In addition, the monitoring system has been reinforced, and new geological surveys have been carried out for the construction of a Frodolfo River by-pass tunnel. In the last few years, the catchment and removal of water from the Confinale stream, combined with a dry period, led to a gradual stabilization of the landslide.

2.2. Monitoring system and previous studies

Currently, the area affected by the Ruinon Landslide is monitored by both, shallow and deep instrumentation, mainly located in the area of the two niches and upstream of the higher one. The monitoring network includes 5 piezometers, extensometers, inclinometers (Fig. 1), and a ground-based interferometric synthetic aperture radar (GBInSAR – Fig. 2). The presence of a well-developed monitoring network provides a large amount of data, and has allowed to carry out several studies on the evolution of the landslide, by analyzing the triggering factors, and leading to the development of an early-warning system. The monitoring system is managed by the Geological Monitoring Center (CMG in italian), belonging to the Sondrio Department of ARPA Lombardia, which has installed the instrumentation and performs periodic campaigns of surveys with manual equipment (dystometric, piezometric, GPS, and inclinometric measurement campaigns).

Initial studies were mainly focused on the definition of volumes and materials involved in the gravitational phenomena (Section 2). Geological and geotechnical investigations began in 1988. Up to date, 34 boreholes have been drilled along the slope. Investigations also included seismic-refraction surveys, geomechanical surveys, and mechanical laboratory tests (e.g., uniaxial compression, direct shear tests) to analyze the elastic and strength properties of the materials.

Agliardi et al. 2001[19] developed a conceptual model regarding the kinematics, age, and state of activity of the Saline DSGSD. Results showed that deformations started after the Late-Wurmian age (15,000 $\pm$ 11,000 years B.P.) and continued until few centuries ago, not excluding a present-day low-rate activity. Numerical modeling indicates post-glacial distress as the main triggering factor of the deep slope deformation.

Crosta and Agliardi 2003[41] applied the generalized method proposed by Voight 1988, 1989,[9,53] to assess the non-linear time-dependent behavior of the Ruinon landslide towards failure, and defining alert velocity thresholds using displacements monitoring data.

The Ruinon landslide was picked as one of the first experimental sites monitored by a GBInSAR system[54,55] that was permanently installed in 2006[56] as a monitoring and early warning tool (Fig. 2a). Ground-based satellite data from years 2006–2007 were analyzed by Del Ventisette et al. 2012,[51] defining a relation between displacements of the landslide body and the rainfall regime. Crosta et al. 2017[43] analyzed 9 years of continuous monitoring activity (2006–2014), identifying "early warning domains" within the landslide body, defined by homogeneous materials, sliding mechanisms and response to rainfall inputs. For each landslide domain, displacement rates and rainfall thresholds were defined. Carlà et al. 2021[52] reviewed more than a decade of GBInSAR data, analyzing the evolution of the slope in both space and time. Starting from displacement data, the thickness of the rapidly moving layer of debris was assessed. The results of the FEM performed by the authors, suggested that the debris cover downslope of the lower scarp is near the limit equilibrium, even in the absence of external forcing, whereas the onset of movements in the upper area are predominantly governed by abrupt rises of piezometric levels. Despite the variability of materials, morphology and activity, every sector of the slope seems to be related to the same driving mechanism. Currently, the GBInSAR consists of 45 target points located along the landslide body, whose distance to the radar instrument is measured continuously with an interval depending on the state of the landslide activity.

Fig. 2b shows the cumulative displacement values of the 2014–2020 period, recorded from four different monitoring points of the GBInSAR system. A continuous deformation of the landslide body, typical of a secondary creep behavior, is quite evident (Fig. 2). Moreover, a seasonal component can also be noted, with a significant increase in deformation rates during the late spring to summer period, in correspondence with substantial rainfall and snowmelt. Two episodes of landslide acceleration are well noticeable during the years of 2016 and 2019, causing rapid shallow gravitational events, as discussed in Section 2.2. By relating the landslide velocity to the trend of groundwater level recorded by the piezometer located close to the landslide body (PZ4), a correlation between pore pressures and the strain rate is apparent (Fig. 2c).

3. Methodology

In this work, a thermo-poro-mechanical model with a 1D approach was developed, and a constitutive equation was implemented to link the pore pressure evolution with the landslide internal response.

The presented model assumes that most of the landslide deformation is concentrated on a basal shear band, representing the sliding surface: the landslide body is considered as a rigid block sliding on a thin visco-plastic shear band that exhibits thermal softening and velocity hardening. When the landslide accelerates, mechanical dissipation occurs due to friction, which raises the basal temperature and reduces the shearing resistance of the shear-band material. This process can continue up to the point when the friction coefficient decreases uncontrollably due to a thermal runaway instability.[30,33] The system is thus forced to become unstable, even when reducing the external driving factors (i.e., decreasing of the groundwater table), as it was shown to occur in the case of the Vajont landslide.[57,58]

The mathematical model and the constitutive equations used to forecast the behavior of this type of landslides were, first, proposed by Vardoulakis 2002b,[59] and further developed, among others, by Veveakis et al. 2007,[30] Cecinato et al. 2011[31] and Seguì et al. 2020.[33] The model was applied to the Vajont landslide (Italy) and to the Shuping landslide (Three Gorges Dam, China), to back analyze their stability and velocity evolution,[33] and to the El Forn Landslide (Andorra) as an early warning tool.[35] In the following sections, the mathematical formulation (already extensively described in Seguì et al. 2020[32] and Seguì 2020[40]) is briefly recalled and the application of the model to the Ruinon case history is presented.

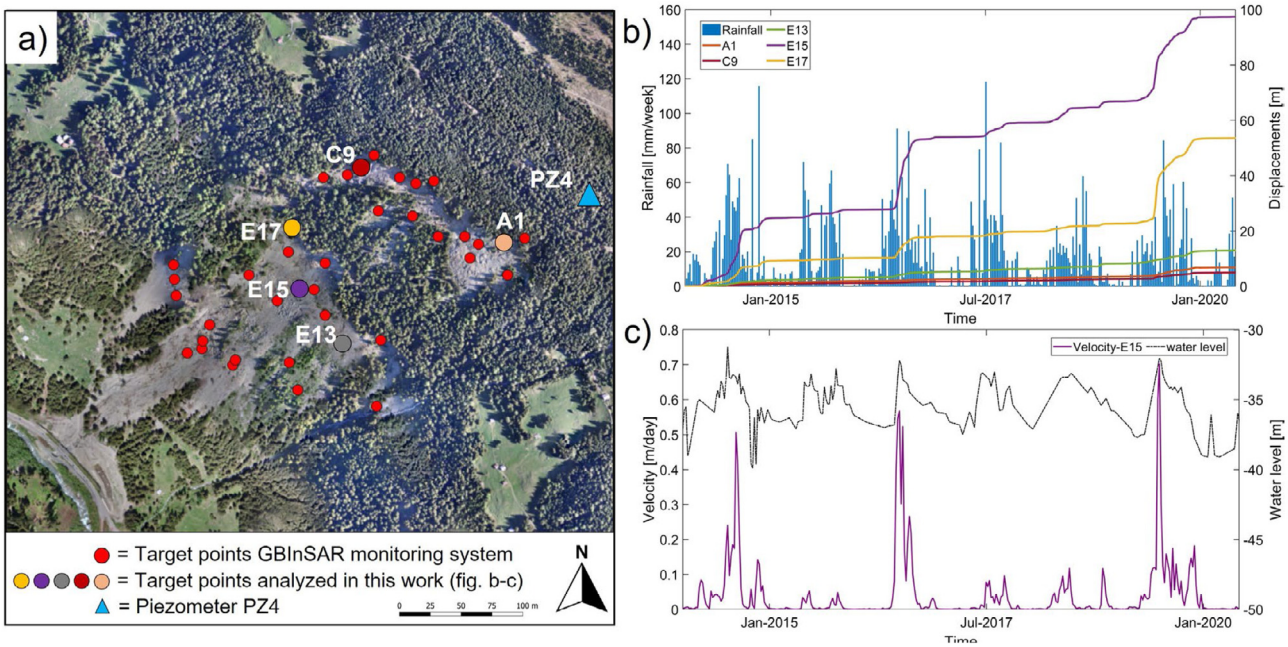

Fig. 2. (a) Location of the target points of the GBInSAR monitoring system; target points analyzed in this work are highlighted with different colors (see the legend). (b) Cumulative displacements and rainfall recorded at the Confinale station (location in Fig. 1). (c) Velocity of the landslide body (E15 point) and evolution of the pore pressure calculated at the sliding surface, based on data collected by piezometer PZ4 (see Section 3.3).

3.1. Mathematical model

Starting from momentum, mass, and energy balance laws, and by assuming that the landslide shear band is fully saturated, without advection and volumetric changes ($\varepsilon_V = \varepsilon_{zz} = 0$), the governing equation describing temperature generation and diffusion within the sliding surface can be defined as:

$$\frac{\partial T}{\partial t} = \alpha \frac{\partial^2 T}{\partial Z^2} + \left(\frac{\tau_d \dot{\gamma}}{\rho C_P}\right) \tag{1}$$

Where $\alpha = K/\rho C_P$ is the thermal diffusivity, ρ is the density, C_P is the specific heat capacity, K is the thermal conductivity of the shear band material, τ_d is the shear stress acting on the sliding surface, $\dot{\gamma}$ is the shear strain rate, and T is temperature.

In Eq. (1), a constitutive response for the irreversible part of the strain-rate needs to be introduced. This is obtained by considering the sliding material to be visco-plastic, exhibiting a thermal and rate sensitivity behavior, following the work of Vardoulakis 2002a[29] and Veveakis et al. 2007.[30] By assuming velocity hardening (the shear strength increases as the shearing velocity increases) and thermal softening (when the temperature increases, the shear strength of the material decreases) the constitutive law for the shearing material can be described by the following expression:

$$\dot{\gamma} = \dot{\gamma}_{ref} \left(\frac{\tau_d}{\tau_{ref}}\right)^{1/N} e^{m(T-T_0)} \tag{2}$$

Where $\dot{\gamma}_{ref}$ is the reference shear strain-rate, τ_{ref} is the reference shear stress, N is the frictional rate-sensitivity coefficient, m is the ratio of the temperature sensitivity coefficient (M) over the strain-rate sensitivity coefficient (N), T is the temperature in the shear band, and T_0 is a reference temperature. Therefore, Eq. (1) can be written as:

$$\frac{\partial T}{\partial t} = \alpha \frac{\partial^2 T}{\partial Z^2} + \left(\frac{\tau_d}{\rho C_P}\right) \dot{\gamma}_{ref} \left(\frac{\tau_d}{\tau_{ref}}\right)^{1/N} e^{m(T-T_0)} \tag{3}$$

Eq. (3) can be reduced to a dimensionless equation by considering the following dimensionless parameters:

$$z^* = z/(0.5 * z)$$
$$t^* = (k_m/(0.5 * ds)^2) * t$$
$$T^* = m(T - T_0)$$

Where, ds is the thickness of the active shear band. Eq. (3) in dimensionless form, becomes:

$$\frac{\partial T^*}{\partial t^*} = \frac{\partial^2 T^*}{\partial Z^{*2}} + Gre^{T^*} \tag{4}$$

where Gr is the Gruntfest number,[34] defined as:

$$Gr = G_0 \left(1 + \frac{P_f}{P_{f0}}\right)^{1+\frac{1}{N}} \tag{5}$$

With:

$$G_0 = m \frac{\dot{\gamma}_{ref}}{\alpha \rho C_P} \frac{ds^2}{4} \tau_{d,ref} \tag{6}$$

where P_f the groundwater pressure and P_{f0} the reference pressure.

The Gruntfest number is a dimensionless parameter that could be considered to act as a link between the external loading conditions and the internal response of the material, since it evolves with the pore water pressure (Eq. (5)), and consequently with time. As shown by Eq. (4), it should be noted that the system depends on a single parameter, Gr, that expresses the ratio of the mechanical work converted into heat over the heat diffusion capabilities of the material. Following the discussion presented in Seguí et al. 2020,[33] the stability assessment of the system can be performed by computing the steady-state response of the dimensionless temperature as a function of the Gruntfest number, through a numerical bifurcation analysis. If the combination of pore pressure (and consequently shear stresses), Gruntfest number and temperature is such that the state of the system remains within the area of stability (green area in Fig. 3), the system has the capacity to diffuse away the heat generated inside the shear

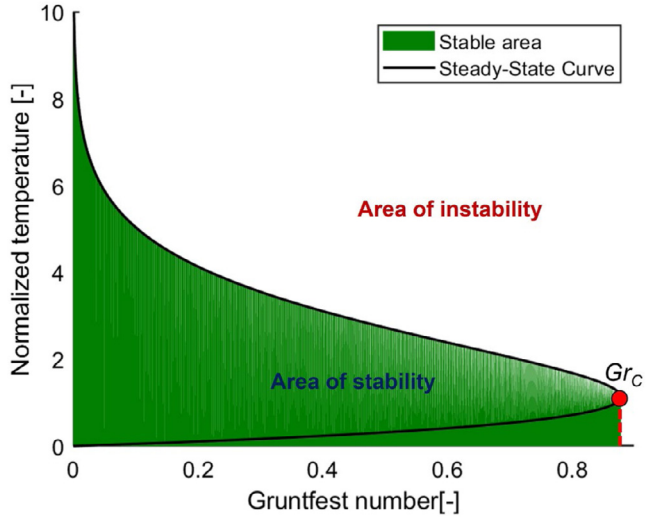

Fig. 3. Representation of the steady-state curve and area of stability of the dimensionless temperature as a function of the Gruntfest number. The value of critical Grunfest is also highlighted in red. A full mathematical discussion can be found in Refs. 30, 33, 34, 60.

band due to friction and maintain a stable, slow creeping. As soon as the shear stress or temperature lead Gr to increase above the critical value (Gr_c), or the (Gr, T) combination to lie outside the area of stability, the system is entering a quasi-adiabatic regime, where the heat generated due to friction cannot be diffused away, causing abrupt increase of the temperature leading to a so-called thermal runaway process.[34]

Once the temperature is calculated by solving Eq. (4), the next step is to determine the velocity, V, and cumulative displacement, u, of the landslide. This is achieved in our model by integrating the strain rate over space and time. For the velocity:

$$V = \int_{-ds/2}^{ds/2} \dot{\gamma}\, dz = V_0 \int_0^1 \left(\frac{P_f}{P_{f0}}\right)^{1/N} e^{T^*} dz^* \tag{7}$$

Where V_0 is the reference velocity of the slope, which can be calculated from the slope displacement data detected outside the main landslide body.

Based on the above presented mathematical formulation, the input data required by the model are the pore pressure, reference stress and velocity, as well as the initial temperature at the shear band and its thickness. In addition, to define the constitutive parameters of the shear band (modeled as a visco-plastic medium with thermal softening and velocity hardening, see Eq. (2)), thermal and load rate sensitivity of the material must be measured or estimated, along with thermal diffusivity and density.

3.2. Laboratory tests: thermal and load rate sensitivity

Experimental tests in a customized triaxial apparatus with velocity and temperature control were performed to explore the Ruinon material behavior and define thermal and load rate sensitivity parameters. Although representative values have been suggested in the literature, they are material sensitive and can only be fully determined through laboratory testing at different loading rates and temperatures. Because of the non-linear dependence of Gr on thermal and load rate sensitivity, the model is extremely sensitive to small variations of their values (especially for N).

The material tested in this framework, was sampled from the rock cores of the boreholes drilled along the Ruinon slope. Since no material is available from the shear band, as the boreholes are located outside the main landslide body, intact rock samples were collected at a depth of about 30 m from the locations closest to the landslide. Geological surveys and stratigraphic analyses have shown lithological homogeneity along the slope, and it is therefore reasonable to assume that the material composing the sliding surface is the same as the main landslide body, only with a different degree of fracturing. From the collected material, 6 cylindrical specimens (38 mm diameter, 75 mm height) were obtained (Fig. 4b). The rock material consists of phyllites with light bands composed of sericite, chlorite and sometimes graphite minerals and quartz bands. Quartz can also be present in veins or lenses.[42,46]

The six available samples were divided into two groups of three samples each, one to be tested for the load rate sensitivity and one for the thermal sensitivity. Load-rate sensitivity tests were conducted in a triaxial machine by applying a confining pressure of 1 MPa and a strain-controlled axial load until the specimen was led to a critical state or failure. Three different loading rates were tested: 0.005, 0.1 and 0.2 mm/min.

Thermal sensitivity tests were carried out by keeping the confining pressure and the loading rate at constant values of 1 MPa and 0.1 mm/min, respectively. During the first step, samples were heated to a specified temperature through a warming process with 3 °C steps, inducing a rate of 1.5 °C per hour before letting it equilibrate. Once the temperature had stabilized, the axial load was increased while keeping the strain rate of 0.1 mm/min constant, and the specimen was brought to failure (step 2). The temperature of the sample was monitored with a thermal probe less than 10 mm away from the sample, and the imposed temperature was held constant until steady-state was achieved in the specimen. Four different temperatures (20, 35, 50 and 80 °C) were tested. By studying the relationship between deviatoric failure stress, temperature (Fig. 4c), and loading velocity (Fig. 4d), the thermal sensitivity ($M = 0.006\ °C^{-1}$) and load rate sensitivity ($N = 0.075$) parameters were obtained. Regarding the results of the rate sensitivity, a power interpolation fitting line was obtained, suggesting a rate hardening behavior of the material. The thermal sensitivity results show an exponential interpolation line, suggesting a thermal softening behavior. These results are in accordance with the analysis conducted by Seguì and Veveakis 2021[35] and Seguì 2020[40] on similar rock materials. Compared with literature values, the tested material showed moderate load rate sensitivity and low thermal sensitivity, probably due to the nature of the material with a poor clay mineral component.

3.3. Model application to the ruinon landslide

Monitoring data presented in Section 2.2 (Fig. 2), showed a marked correlation between landslide velocities and pore pressure variations. In this section, the thermo-poro-mechanical mathematical model, combined with the constitutive law calibrated with the laboratory test results (rate and thermal sensitivities), is applied to the Ruinon landslide.

The input data required by the model are represented by pore pressure values at the sliding surface, together with the shear band material properties. Hydraulic load values measured by the piezometer located at the high niche of the landslide (Fig. 2a) were used to calculate the pore pressure values by the relation $P_f = gH\rho_w$ (where g is the gravity acceleration, H the water head, and ρ_w the water density). From previous studies, in fact, it can be assumed that the shallow aquifer (Fig. 2) located in the sliding mass is responsible for the development of pore water pressures along the sliding surface. Considering the stratigraphic log data, a slip surface of 80 meters depth was assumed, and pore pressures were calculated in hydrostatic conditions considering the piezometric head above the sliding surface (Fig. 5).

Sample	Axial load [mm/min]	Temperature [°C]
A	0.005	20
B	0.1	20
C	0.2	20
D	0.1	35
E	0.1	50
F	0.1	80

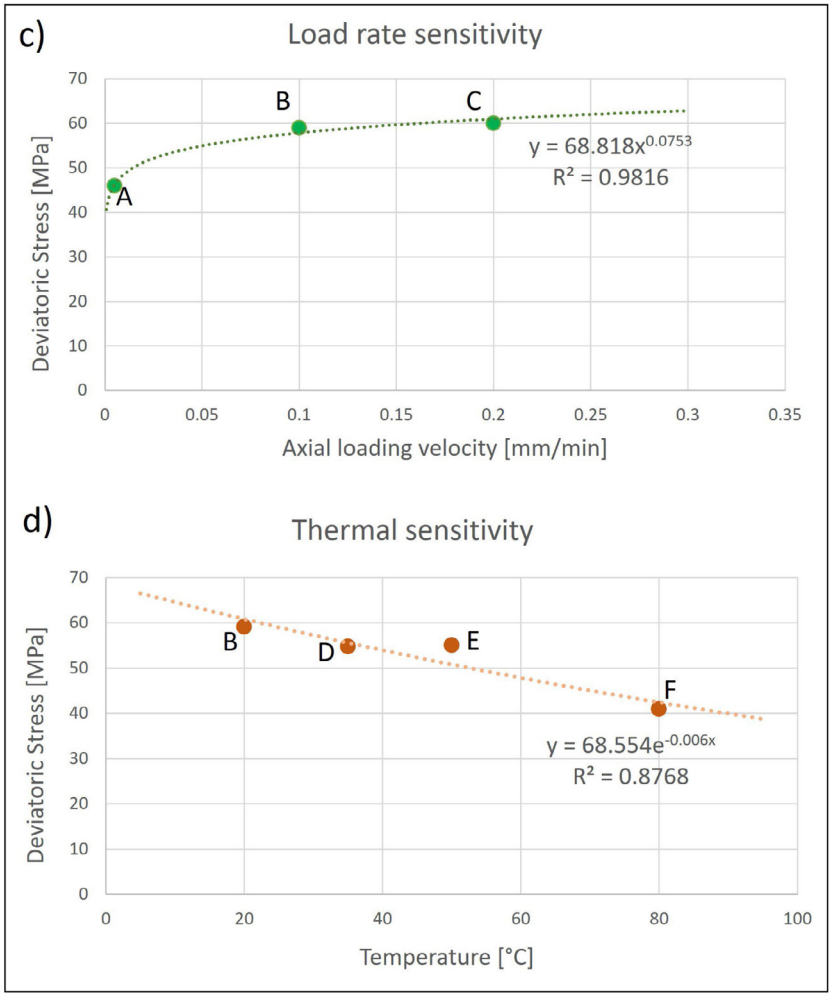

Fig. 4. (a) Values of axial loads and temperature applied to the rock samples tested in a triaxial cell with a confinement pressure of 1 MPa. (b) Example of sample tested in the triaxial cell. (c) Relation detected between deviatoric failure stress and axial loads. (d) Relation detected between deviatoric failure stress and temperature.

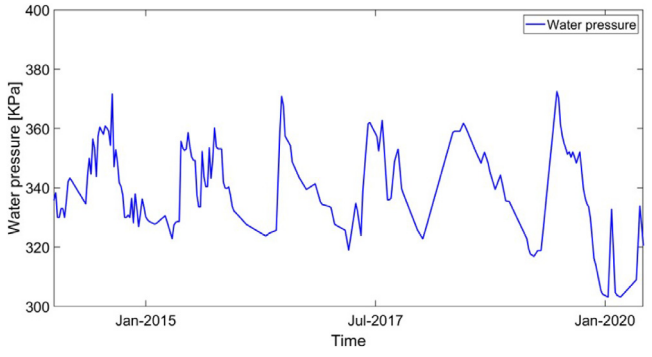

Fig. 5. Pore pressure data introduced as input factor for the analysis.

A reference temperature value of 10 °C was defined, which can be considered a representative average annual value for the slope at the considered sliding depths. This value agrees with the water temperatures measured at the springs around the "low niche". The thermal and mechanical parameters of the material derived from both laboratory tests (Section 3.2) and the literature, are presented in Table 1.

Having constrained the above values, the remaining parameters required in the expression of *Gr* are the reference values of the loading stress, and the active shear band thickness, *ds*. Both quantities cannot be easily determined from field data. To constrain the loading stress, results from the regional FEM stress–strain model presented in Morcioni et al. 2023[44] were introduced. At a depth of about 80 m, the model indicates shear stresses in a range of 0.2–0.5 MPa that were used as reference values (τ_{ref}). In addition, the results of 3D stress–strain modeling presented in Part 1 of this study,[44] allowed us to assess the time-dependent evolution of the shear stress with piezometric level. Through FEM modeling, by comparing effective stress values for different groundwater scenarios, a linear relationship was obtained. This allowed, as a first approximation, to introduce a simple linear equation to calculate the stress state along the slip surface of the landslide, depending only on the depth of the groundwater table.

Concerning the thickness of the active shear band, an initial value of 0.1 m was assumed, based on stratigraphic and geological data (see Section 2). Then, the thermal sensitivity coefficient *M* and the reference values of the stress were used to infer the shear thickness value through an inversion analysis,[33] described in Section 4. The modeling analysis was divided into two different steps. In a first step defined "training step", the pore pressure data relevant to the years 2014–2018 were introduced as input factors. This step allowed to calibrate the model, by comparing the outputs of the model with the displacement and velocity data recorded by the landslide monitoring system. The normalized

Table 1
Material parameters of the Ruinon shear band.

Parameter	Value	Detection method
Load rate sensitivity (N)	0.075	Laboratory test
Thermal sensitivity (M)	0.006 °C^{-1}	Laboratory test
Thermal diffusivity (α)	6e^{-7} (m^2/s)	Cermak and Rybach 1982[61]
Density (ρ)	2700 (Kg/m^3)	Griffini 2004[42]
Heat capacity (C_P)	910 (J/Kg*K)	Cermak and Rybach 1982[61]
Thermal conductivity (K)	1.5 (W/(m*K))	Cermak and Rybach 1982[61]
Reference slope velocity (V_0)	0.018 m/yr	In-situ monitoring system
Reference stresses (τ_{ref})	2e5 Pa	Stress–strain modeling- Part1
Reference temperature (T_{ref})	10 °C	Assumption based on in-situ observations
Active shear band thickness (ds)	0.1 m	Inversion analysis - calibration
Initial Gruntfest number (G_0)	2e−5	Inversion analysis - calibration

field data were fitted by the model calculated velocity using the time-dependent Gr number as an inversion parameter. Once the model was calibrated, defining G_0 and ds, the second step of the analysis involved the prediction of velocities by introducing pore pressure values relevant to years 2018–2020. To validate the model, calculated output velocities were compared to the normalized field data recorded by the GBInSAR system, which provided a sufficiently large dataset. Point E15 (Fig. 2) was taken as a reference because: (i) the location of this station represents the center of mass of the landslide, and (ii) it exhibits the largest displacements, which allows us to evaluate the slope stability for the worst-case scenario. The choice of taking velocity data recorded at the slope surface as representative of the slope assumes the landslide mass to move as a rigid body with no change in velocity from the shear band to the topographic surface, as required by the model. This may be seen as a strong assumption and a limitation of the adopted approach, but it allows to perform a conservative analysis. In fact, all risk protection and mitigation actions refer to surface velocity values of the landslide body, which typically exhibit a similar trend to the deep ones but with higher magnitudes. Thus, simulating surface velocities allows us to directly plan risk protection and mitigation activities, representing an advantage, especially considering the possibility to forecast future landslide evolutions.

4. Results

Model outputs were analyzed in terms of simulated velocity trends and Gruntfest number evolution, in relation to pore pressure inputs and the associated curve of stability.

In a first step the model was calibrated, based on the comparison between modeled velocities and velocity data recorded by the monitoring system in the period January 2014–January 2018. All parameters required by the model were calibrated by identifying the best fitting between simulated and monitored landslide velocity in the above stated period (Fig. 6a). In this phase, the Gruntfest number was constrained by an inverse analysis: although all parameters that define Gr are known, an assumption for G_0 is necessary.

Different values of G_0 were thus hypothesized, and a value of 2e-5 was defined as the one providing the best velocity fitting (Fig. 6a). Moreover, the thickness of the shear band (ds) was constrained by solving Eq. (6) as a function of ds. Considering the best-fit value of G_0, Eq. (6) was applied to invert for the shear band thickness (ds) and the driving background stress ($\tau_{d,ref}$). Using a range of thermal sensitivity (M) values, different relations between $\tau_{d,ref}$ and ds were obtained (Fig. 6b). Fixing the thermal sensitivity by considering the results of laboratory tests (Section 3.1), a value of ds could be defined in the plot by constraining the reference shear stresses. A $\tau_{d,ref}$ interval of 0.2–0.5 MPa acting on the sliding surface was defined based on results of the regional FEM modeling, presented in Part 1 of this work.[44] By evaluating the relationship between all the factors introduced in the plot of Fig. 6b, a shear band thickness of 0.1 meters was obtained.

Once calibrated, the model was validated over the years 2018–2020, without changing the values defined in the calibration step. As can be seen in Fig. 7c, a good correspondence between recorded and simulated values of velocity was obtained.

Deviations between the two curves in Fig. 7c are mainly defined by differences in the magnitude and amplitude of a few velocity peaks. However, in general, the model reproduces with accuracy the landslide behavior, by correctly identifying periods of maximum acceleration of the sliding mass. The relationship between groundwater level trends and landslide velocity is well reproduced. Fig. 7a and b respectively show the evaluated Gruntfest number (Gr) against normalized temperature in the model's phase space and the basal temperature over time.

Fig. 7a shows that Gr and temperature vary along the lower branch of the stable curve (i.e., within the stable area of the graph) with values close to the unstable area of the phase-space, but never reaching it, hence the landslide remains stable in the secondary creep phase. This agrees with the monitored evolution of the landslide, exhibiting near-collapse conditions with significant accelerations and very frequent gravitational events (Section 2.1). The calculated basal temperature (Fig. 7c) follows the evolution of the shear stresses (and consequently the pore pressures) acting along the slip surface. It varies over a range of about 5 degrees, with maximum temperature peaks corresponding to pore pressure peaks. During the years 2016 and 2019, a significant landslide acceleration event occurred, in correspondence with a sudden increase in the piezometric level. This also resulted in a rise of the basal temperature, due to the increase of frictional heat, which may have modified the internal mechanical conditions and exacerbated the velocity values.

5. Discussion and conclusions

In this work, a physics-based mathematical model was applied to the Ruinon landslide, allowing the simulation of the displacement history recorded by a bespoke geotechnical monitoring system. The model combines external and internal factors that control the landslide evolution, through the definition of the so-called Gruntfest number. The pore pressure evolution (causing a basal shear stress evolution), due to groundwater fluctuations, represents the main external driving factor for the landslide, while the mechanical weakening of the shear band, due to loading rate and temperature variations, defines its internal response.

Considering the time-period covered by the analysis, stable conditions are simulated by the model. Gr values, however, evolve close to critical stability in the model phase space, in accordance with field observations and previous work that showed

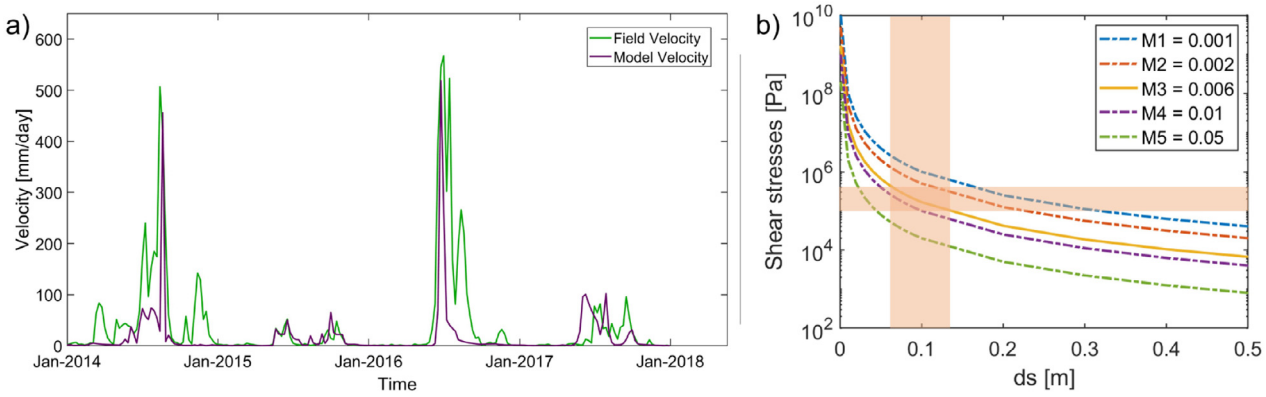

Fig. 6. Model calibration analysis. (a) Best fitting obtained between modeled and monitored velocities. (b) Evolution of the shear stress in relation to the active shear band thickness, with different scenarios of thermal sensitivity (M). Fixing the thermal sensitivity value by considering the results of laboratory tests ($M = 0.006$), a value of ds was defined by constraining the reference shear stresses on results of the regional FEM modeling.

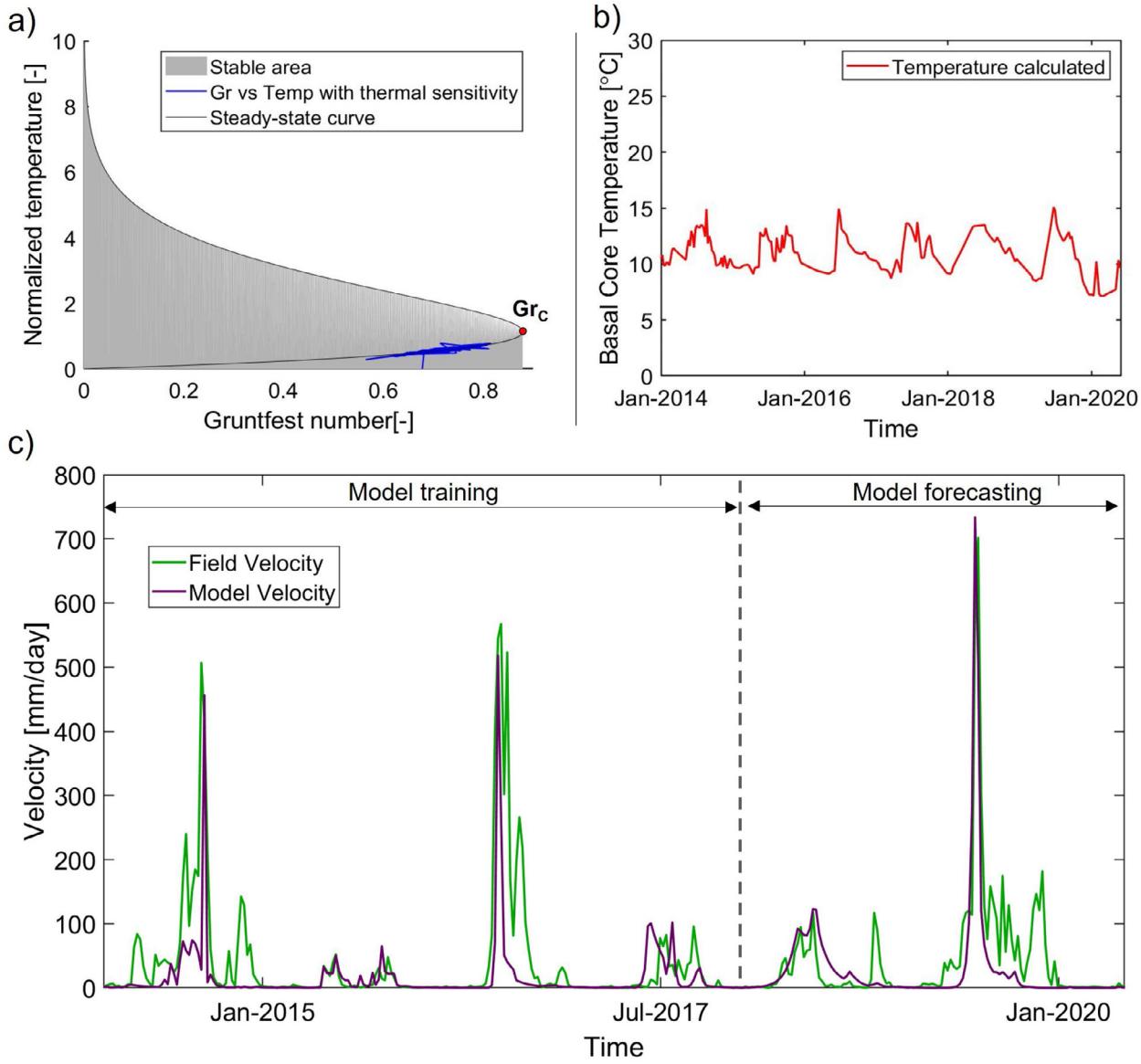

Fig. 7. (a) Evolution of the Gruntfest number and the modeled temperature (b). (c) Validation of the model by predicting velocities for the years 2018–2020 and comparing them with the monitored ones.

a significant landslide activity with displacements and velocity values close to a critical point (i.e., close to tertiary creep, or final acceleration of the landslide, representing catastrophic collapse). By way of example, velocity thresholds identified by Crosta and Agliardi 2003[41] were exceeded several times at the monitored point, during the 2014, 2016, and 2019 events.

Deviations between the calculated and monitored velocities are shown in this study, and a slight difference between the two can be noted in terms of magnitude and time lag, especially at the velocity peaks. This may be explained considering the one-dimensional approach of the presented analysis, which neglects the natural 2- and 3-D evolution of the stresses. Moreover, in this work, field velocities are relevant to a monitoring point located on the surface of the landslide body, that can be affected by secondary shallow accelerations, which are neglected by this modeling approach. However, considering all the necessary assumptions made in the mathematical model, the results obtained can be considered to faithfully simulate the general behavior of the landslide, by properly matching the velocity peaks and their time of occurrence. In fact, the landslide sliding behavior and its relationship with the pore pressure evolution was well reproduced.

Another uncertainty factor may be represented by the temperature calculated at the sliding surface, as no monitoring data for this parameter are available. However, the reference temperature (T_0) of 10 °C is sufficiently representative of the slope under analysis, consistently with water temperature data recorded at springs near the lower landslide niche. This value is also in agreement with temperatures calculated in previous works, where the thermal evolution along an Alpine slope was simulated in similar geological and morphological conditions.[62,63] Future numerical simulations of the entire slope could be performed to include thermal diffusion and groundwater-driven convection processes to better define the boundary temperature values at the sliding surface.

The parameters used in the model (listed in Table 1) are in line with realistic ranges reported in the literature. Concerning the values of G_0 and *ds* (which are the most uncertain parameters, as they cannot be directly measured or easily estimated), they were constrained through a calibration process, involving inverse analysis until the best match between modeled and measured velocities was achieved. The only way to better constrain G_0 would be to obtain temperature monitoring values at the sliding surface, as shown by Seguí and Veveakis 2021,[35] and define a statistical distribution analysis to identify the best fitting between the calculated temperature and the monitored one. Monitoring the temperature along the slip surface would lead to greater reliability of the model. In addition, temperature monitoring would allow us to check the real-time stability condition of the landslide and continuously assess its positioning in the stability phase-space (see Fig. 7). A key feature of the presented analysis lies in the consequentiality between the output of the regional FEM model[44] and the input of the present analysis. In fact, a linear relation between the shear stress and the groundwater level was identified[44] and introduced to define the reference effective stress state along the sliding surface.

This model represents an innovative physics-based tool to analyze the behavior of landslides and could constitute the basis of a landslide early-warning system, used in combination with traditional monitoring methods. The key feature of this model is that it accounts for the thermal and velocity sensitivities of the shear band material, as well as the effect of pore pressure in promoting the evolution of different creeping stages. Once validated with field data, the model can be also used as a real-time assessment tool, to forecast the behavior of large deep-seated landslides, especially considering future climate change scenarios. In future developments of the analysis, regional climate models can be used to obtain climate projected data for the Ruinon area. The long-term temperature and pore pressure evolution along the slope, with particular reference to the depth of the sliding surface, can be forecasted and used in the model to verify their influence on the landslide behavior.

The robustness of the modeling approach proposed by Seguì et al. 2020,[33] Seguì 2020,[40] Seguì and Veveakis 2021[35] has been demonstrated in this work, by applying the model to a different geological, geomorphological, and geomechanical setting. The main advantage of this approach is that it allows for a physics-based solution, by requiring relatively few input parameters, which can be easily obtained from the literature in the absence of direct measurements. The presented approach may soon be applied to further case studies, aimed at the definition of a novel physics-based early warning tool for landslides.

CRediT authorship contribution statement

Andrea Morcioni: Conceptualization, Methodology, Data curation, Software, Formal analysis, Writing – original draft. **Tiziana Apuani:** Visualization, Data curation, Supervision, Writing – reviewing & editing. **Francesco Cecinato:** Visualization, Data curation, Supervision, Writing – reviewing & editing. **Manolis Veveakis:** Methodology, Validation, Visualization, Supervision, Writing – reviewing & editing.

Declaration of competing interest

The authors declare that they have no known competing financial interests or personal relationships that could have appeared to influence the work reported in this paper.

Data availability

Data will be made available on request.

Acknowledgments

This research has been carried out in the framework of the Doctoral Program in Earth Sciences of the University of Milan and supported by the NSF CMMI-2042325 award. The Authors are also grateful to ARPA Lombardia for making the field monitoring data available.

References

1. Fellenius W. Calculation of the stability of earth dams. In: *Proc 2nd Congr Large Dams. Vol. 4.* 1936:445–462.
2. Bishop AW. The use of the slip circle in the stability analysis of slopes. *Géotechnique*. 1955;5(1):7–17. http://dx.doi.org/10.1680/geot.1955.5.1.7.
3. Morgenstern NR, Price VE. The analysis of the stability of general slip surfaces. *Géotechnique*. 1965;15(1):79–93. http://dx.doi.org/10.1680/geot.1965.15.1.79.
4. Spencer E. A method of analysis of the stability of embankments assuming parallel inter-slice forces. *Géotechnique*. 1967;17(1):11–26. http://dx.doi.org/10.1680/geot.1967.17.1.11.
5. Janbu N. *Slope Stability Computations*. Publ Wiley Sons, Inc; 1973 Published online.
6. Chen Z-Y, Morgenstern NR. Extensions to the generalized method of slices for stability analysis. *Can Geotech J*. 1983;20(1):104–119. http://dx.doi.org/10.1139/t83-010.
7. Saito M. Forecasting the time of occurrence of a slope failure. In: *Proc 6 th Int Conf Soil Mech Found Eng*. 1965:537–541. Published online https://cir.nii.ac.jp/crid/1572543024011185664.bib?lang=ja.
8. Saito M. Forecasting time of slope failure by tertiary creep. In: *Proceedings of the 7th International Conference on Soil Mechanics and Foundation Engineering, Mexico City, Mexico. Vol 2.* 1969:677–683.
9. Voight B. A method for prediction of volcanic eruptions. *Nature*. 1988;332(6160):125–130. http://dx.doi.org/10.1038/332125a0.

10. Helmstetter A, Sornette D, Grasso J-R, Andersen JV, Gluzman S, Pisarenko V. Slider block friction model for landslides: Application to Vaiont and La Clapière landslides. *J Geophys Res Solid Earth*. 2004;109(B2):1–15. http://dx.doi.org/10.1029/2002jb002160.
11. Sornette D, Helmstetter A, Andersen JV, Gluzman S, Grasso JR, Pisarenko V. Towards landslide predictions: Two case studies. *Phys A Stat Mech its Appl*. 2004;338(3–4):605–632. http://dx.doi.org/10.1016/j.physa.2004.02.065.
12. Eberhardt E. Twenty-ninth Canadian Geotechnical Colloquium: The role of advanced numerical methods and geotechnical field measurements in understanding complex deep-seated rock slope failure mechanisms. *Can Geotech J*. 2008;45(4):484–510. http://dx.doi.org/10.1139/T07-116.
13. Preisig G, Eberhardt E, Smithyman M, Preh A, Bonzanigo L. Hydromechanical rock mass fatigue in deep-seated landslides accompanying seasonal variations in pore pressures. *Rock Mech Rock Eng*. 2016;49(6):2333–2351. http://dx.doi.org/10.1007/s00603-016-0912-5.
14. Cappa F, Guglielmi Y, Soukatchoff VM, Mudry J, Bertr C, Charmoille A. Hydromechanical modeling of a large moving rock slope inferred from slope levelling coupled to spring long-term hydrochemical monitoring: Example of the La Clapière landslide (Southern Alps, France). *J Hydrol*. 2004;291(1–2):67–90. http://dx.doi.org/10.1016/j.jhydrol.2003.12.013.
15. Gunzburger Y, Merrien-Soukatchoff V, Guglielmi Y. Influence of daily surface temperature fluctuations on rock slope stability: Case study of the Rochers de Valabres slope (France). *Int J Rock Mech Min Sci*. 2005;42(3):331–349. http://dx.doi.org/10.1016/j.ijrmms.2004.11.003.
16. Zangerl C, Eberhardt E, Perzlmaier S. Kinematic behaviour and velocity characteristics of a complex deep-seated crystalline rockslide system in relation to its interaction with a dam reservoir. *Eng Geol*. 2010;112(1–4):53–67. http://dx.doi.org/10.1016/j.enggeo.2010.01.001.
17. Crosta GB, di Prisco C, Frattini P, Frigerio G, Castellanza R, Agliardi F. Chasing a complete understanding of the triggering mechanisms of a large rapidly evolving rockslide. *Landslides*. 2013;11(5):747–764. http://dx.doi.org/10.1007/s10346-013-0433-1.
18. Morcioni A, Apuani T, Cecinato F. Piuro landslide: 3D hydromechanical numerical modelling of the 1618 event. *Geoscience*. 2023;13(2). http://dx.doi.org/10.3390/geosciences13020049.
19. Agliardi F, Crosta G, Zanchi A. Structural constraints on deep-seated slope deformation kinematics. *Eng Geol*. 2001;59(1–2):83–102. http://dx.doi.org/10.1016/S0013-7952(00)00066-1.
20. Eberhardt E, Stead D, Coggan JS. Numerical analysis of initiation and progressive failure in natural rock slopes-the 1991 Randa rockslide. *Int J Rock Mech Min Sci*. 2004;41(1):69–87. http://dx.doi.org/10.1016/S1365-1609(03)00076-5.
21. Ambrosi C, Crosta GB. Large sackung along major tectonic features in the Central Italian Alps. *Eng Geol*. 2006;83(1–3):183–200. http://dx.doi.org/10.1016/j.enggeo.2005.06.031.
22. Apuani T, Masetti M, Rossi M. Stress–strain-time numerical modelling of a deep-seated gravitational slope deformation: Preliminary results. *Quat Int*. 2007;171-172(SPEC. ISS.):80–89. http://dx.doi.org/10.1016/j.quaint.2007.01.014.
23. Agliardi F, Crosta GB, Frattini P, Malusà MG. Giant non-catastrophic landslides and the long-term exhumation of the European Alps. *Earth Planet Sci Lett*. 2013;365:263–274. http://dx.doi.org/10.1016/j.epsl.2013.01.030.
24. Tibaldi A, Pasquarè F. Quaternary deformations along the 'Engadine–Gruf tectonic system', Swiss–Italian Alps. *J Quat Sci*. 2009;22(2008):311–320. http://dx.doi.org/10.1002/jqs.
25. Alonso EE, Zervos A, Pinyol NM. Thermo-poro-mechanical analysis of landslides: from creeping behaviour to catastrophic failure. *Géotechnique*. 2016;66(3):202–219. http://dx.doi.org/10.1680/jgeot.15.LM.006.
26. Goren L, Aharonov E. Long runout landslides: The role of frictional heating and hydraulic diffusivity. *Geophys Res Lett*. 2007;34(7):1–7. http://dx.doi.org/10.1029/2006GL028895.
27. Goren L, Aharonov E, Anders MH. The long runout of the heart mountain landslide: Heating, pressurization, and carbonate decomposition. *J Geophys Res Solid Earth*. 2010;115(10):1–15. http://dx.doi.org/10.1029/2009JB007113.
28. Pinyol NM, Alonso EE. Criteria for rapid sliding II. Thermo-hydro-mechanical and scale effects in Vaiont case. *Eng Geol*. 2010;114(3–4):211–227. http://dx.doi.org/10.1016/j.enggeo.2010.04.017.
29. Vardoulakis I. Steady shear and thermal run-away in clayey gouges. *Int J Solids Struct*. 2002;39(13–14):3831–3844. http://dx.doi.org/10.1016/S0020-7683(02)00179-8.
30. Veveakis E, Vardoulakis I, Di Toro G. Thermoporomechanics of creeping landslides: The 1963 Vaiont slide, northern Italy. *J Geophys Res: Earth Surf*. 2007;112(3):1–21. http://dx.doi.org/10.1029/2006JF000702.
31. Cecinato F, Zervos A. Influence of thermomechanics in the catastrophic collapse of planar landslides. *Can Geotech J*. 2012;49(2):207–225. http://dx.doi.org/10.1139/t11-095.
32. De Blasio FV, Medici L. Microscopic model of rock melting beneath landslides calibrated on the mineralogical analysis of the Köfels frictionite. *Landslides*. 2017;14(1):337–350. http://dx.doi.org/10.1007/s10346-016-0700-z.
33. Seguí C, Rattez H, Veveakis M. On the stability of deep-seated landslides. The cases of vaiont (Italy) and Shuping (Three Gorges Dam, China). *J Geophys Res: Earth Surf*. 2020;125(7):1–24. http://dx.doi.org/10.1029/2019JF005203.
34. Gruntfest IJ. Thermal feedback in liquid flow; Plane shear at constant stress. *Trans Soc Rheol*. 1963;7(1):195–207. http://dx.doi.org/10.1122/1.548954.
35. Seguí C, Veveakis M. Continuous assessment of landslides by measuring their basal temperature. *Landslides*. 2021;18(12):3953–3961. http://dx.doi.org/10.1007/s10346-021-01762-x.
36. Hueckel T, François B, Laloui L. Explaining thermal failure in saturated clays. *Géotechnique*. 2009;59(3):197–212. http://dx.doi.org/10.1680/geot.2009.59.3.197.
37. Ferri F, Di Toro G, Hirose T, Shimamoto T. Evidence of thermal pressurization in high-velocity friction experiments on smectite-rich gouges. *Terra Nov*. 2010;22(5):347–353. http://dx.doi.org/10.1111/j.1365-3121.2010.00955.x.
38. Cappa F, Scuderi MM, Collettini C, Guglielmi Y, Avouac J-P. Stabilization of fault slip by fluid injection in the laboratory and in situ. *Sci Adv*. 2019;5(3):eaau4065. http://dx.doi.org/10.1126/sciadv.aau4065.
39. Bohloli B, Soldal M, Smith H, Skurtveit E, Choi JC, Sauvin G. Frictional properties and seismogenic potential of caprock shales. *Energies*. 2020;13(23). http://dx.doi.org/10.3390/en13236275.
40. Seguí C. Analysis of the stability and response of deep-seated landslides by monitoring their basal temperature. 2020 Published online. https://hdl.handle.net/10161/22193.
41. Crosta GB, Agliardi F. Failure forecast for large rock slides by surface displacement measurements. *Can Geotech J*. 2003;40(1):176–191. http://dx.doi.org/10.1139/t02-085.
42. Griffini L. Valutazione delle condizioni di stabilità della frana del Ruinon e aree limitrofe. 2004 Published online.
43. Crosta GB, Agliardi F, Rivolta C, Alberti S, Dei Cas L. Long-term evolution and early warning strategies for complex rockslides by real-time monitoring. *Landslides*. 2017;14(5):1615–1632. http://dx.doi.org/10.1007/s10346-017-0817-8.
44. Morcioni A, Apuani T, Cecinato F, Veveakis M. Landslide susceptibility evaluation in Alpine environment: 1. 3D Finite Element modeling of the Ruinon (IT) case study. *Geomech Energy Environ*. 2023:100493. http://dx.doi.org/10.1016/j.gete.2023.100493.
45. Crosta G, Zanchi A. Deep seated slope deformations: huge, extraordinary, enigmatic phenomena. In: *Landslides in Research, Theory and Practice, Vol. 1*. 2000:351–358. http://dx.doi.org/10.1680/lirtapv1.34617.0058.
46. Montrasio A, Berra F, Cariboni M, et al Note illustrative della Carta Geologica d'Italia alla scala 1:50.000 - Foglio Bormio. Istituto Superiore per la Protezione e la Ricerca Ambientale Servizio Geologico d'Italia Organo cartografico dello Stato. Published online 1990.
47. Bonsignore G, Borgo A, Gelati R, et al Note illustrative della Carta Geologica d'Italia, Foglio 8—Bormio. In: *Serv Geol d'Italia, Roma*. 1969 Published online.
48. Conti P, MANATscHAL Ganre, Pfister M. Synrift sedimentation, Jurassic and Alpine tectonics in the central Ortler nappe (Eastern Alps, Italy). *Eclogae Geol Helv*. 1994;87(1):63–90.
49. Froitzneim N, Manatschal G. Kinematics of Jurassic rifting, mantle exhumation, and passive-margin formation in the Austroalpine and Penninic nappes (eastern Switzerland). *Bull Geol Soc Am*. 1996;108(9):1120–1133. http://dx.doi.org/10.1130/0016-7606(1996)108.
50. Gregnanin A, Valle M. Deformation and metamorphism in the Austroalpine Oetztal-Stubai Complex (Part II); Early-Alpine evolution in basement and cover. *Ital J Geosci*. 1995;114(2):393–409.
51. Del Ventisette C, Casagli N, Fortuny-Guasch J, Tarchi D. Ruinon landslide (Valfurva, Italy) activity in relation to rainfall by means of GBInSAR monitoring. *Landslides*. 2012;9(4):497–509. http://dx.doi.org/10.1007/s10346-011-0307-3.
52. Carlà T, Gigli G, Lombardi L, Nocentini M, Casagli N. Monitoring and analysis of the exceptional displacements affecting debris at the top of a highly disaggregated rockslide. *Eng Geol*. 2021;294. http://dx.doi.org/10.1016/j.enggeo.2021.106345.
53. Voight B. A relation to describe rate-dependent material failure. *Science (80-)*. 1989;243(4888):200–203. http://dx.doi.org/10.1126/science.243.4888.200.
54. Canuti P, Casagli N, Catani F, Fanti R. Hydrogeological hazard and risk in archaeological sites: Some case studies in Italy. *J Cult Herit*. 2000;1(2):117–125. http://dx.doi.org/10.1016/S1296-2074(00)00158-8.
55. Tarchi D, Casagli N, Fanti R, et al <Tarchi, others, - 2003 - Landslide monitoring by using ground-based SAR interferometry an example of application to the Tessina landsli(2).pdf>. 68 (2003) 15-30.
56. Casagli N, Catani F, Del Ventisette C, Luzi G. Monitoring, prediction, and early warning using ground-based radar interferometry. *Landslides*. 2010;7(3):291–301. http://dx.doi.org/10.1007/s10346-010-0215-y.

57. M L. The rock slide in the Vaiont valley. *Felsmech Ingenoirgeol.* 1964;2:148–212.
58. M L. New considerations on the Vaiont slide. *Felsmech Ingenoirgeol.* 1968;6:1–91.
59. Vardoulakis I. Dynamic thermo-poro-mechanical analysis of catastrophic landslides. *Géotechnique*. 2002;52(3):157–171. http://dx.doi.org/10.1680/geot.2002.52.3.157.
60. Veveakis E, Alevizos S, Vardoulakis I. Chemical reaction capping of thermal instabilities during shear of frictional faults. *J Mech Phys Solids*. 2010;58(9):1175–1194. http://dx.doi.org/10.1016/j.jmps.2010.06.010.
61. Cermak V, Rybach L. Thermal conductivity and specific heat of minerals and rocks. Landolt-Börnstein, New Ser Gr V. 1982:305–343. http://dx.doi.org/10.1007/10201894_62, Published online,
62. Morcioni A, Apuani T, Cecinato F. The role of temperature in the stress–strain evolution of alpine rock-slopes: Thermo-mechanical modelling of the cimaganda rockslide. *Rock Mech Rock Eng*. 2022;55(4):2149–2172. http://dx.doi.org/10.1007/s00603-022-02786-y.
63. Grämiger LM, Moore JR, Gischig VS, Loew S. Thermomechanical stresses drive damage of alpine valley rock walls during repeat glacial cycles. *J Geophys Res: Earth Surf*. 2018;123(10):2620–2646. http://dx.doi.org/10.1029/2018JF004626.